5-5-2012

Improved Tumor Contrast Achieved by Single Time Point Dual-Reporter Fluorescence Imaging

Kenneth M. Tichauer
Dartmouth College

Kimberley S. Samkoe
Dartmouth College

Kristian J. Sexton
Dartmouth College

Jason R. Gunn
Dartmouth College

Tayyaba Hasan
Dartmouth College

See next page for additional authors

Journal of Biomedical Optics

SPIEDigitalLibrary.org/jbo

Improved tumor contrast achieved by single time point dual-reporter fluorescence imaging

Kenneth M. Tichauer
Kimberley S. Samkoe
Kristian J. Sexton
Jason R. Gunn
Tayyaba Hasan
Brian W. Pogue

SPIE

Improved tumor contrast achieved by single time point dual-reporter fluorescence imaging

Kenneth M. Tichauer,[a] Kimberley S. Samkoe,[a,b] Kristian J. Sexton,[a] Jason R. Gunn,[a] Tayyaba Hasan,[c] and Brian W. Pogue[a,b,c]
[a]Dartmouth College, Thayer School of Engineering, Hanover, New Hampshire 03755
[b]Dartmouth Medical School, Department of Surgery, Lebanon, New Hampshire 03756
[c]Massachusetts General Hospital, Wellman Center for Photomedicine, Boston, Massachusetts 02114

Abstract. In this study, we demonstrate a method to quantify biomarker expression that uses an exogenous dual-reporter imaging approach to improve tumor signal detection. The uptake of two fluorophores, one nonspecific and one targeted to the epidermal growth factor receptor (EGFR), were imaged at 1 h in three types of xenograft tumors spanning a range of EGFR expression levels ($n = 6$ in each group). Using this dual-reporter imaging methodology, tumor contrast-to-noise ratio was amplified by >6 times at 1 h postinjection and >2 times at 24 h. Furthermore, by as early as 20 min postinjection, the dual-reporter imaging signal in the tumor correlated significantly with a validated marker of receptor density ($P < 0.05$, $r = 0.93$). Dual-reporter imaging can improve sensitivity and specificity over conventional fluorescence imaging in applications such as fluorescence-guided surgery and directly approximates the receptor status of the tumor, a measure that could be used to inform choices of biological therapies. [DOI: 10.1117/1.JBO.17.6.066001]

Keywords: binding potential; epidermal growth factor receptor; fluorescence; receptor; xenograft; molecular imaging; cancer.

Paper 11712 received Dec. 1, 2011; revised manuscript received Apr. 10, 2012; accepted for publication Apr. 11, 2012; published online Jun. 5, 2012.

1 Introduction

Targeted fluorescent imaging reporters are being used to an ever-greater extent in surgical oncology as a means of improving tumor contrast to guide resection or highlight sensitive tissues that should be avoided.[1,2] The promise of fluorescence-guided surgery to reduce morbidity and mortality has stimulated a number of clinical studies and clinical trials focused on the surgical treatment of oncological pathologies.[3–9] To date, the vast majority of these applications have employed clinically approved fluorescent reporters, which has somewhat limited the number of pathologies to which fluorescence-guided surgery has been applied. However, there is a large and growing number of targeted fluorescent agents that have been employed and presented in preclinical studies,[10] and as the field matures, more and more of these targeted reporters will become clinically available. As they do become available, it will be important to determine optimal procedures for imaging their uptake.

The most obvious approach to imaging targeted fluorescence uptake in tumors is to inject the reporter systemically and then wait several hours or days before imaging. The exact delay time between injection and imaging is ideally chosen to allow nonspecific tissue uptake of the fluorescent reporter to wash away, as well as to allow the reporter to be filtered out of the bloodstream, providing better contrast for reporter that is presumably bound to disease-specific receptors in cancerous lesions. At later times, however, uptake is typically governed more by the enhanced permeability and retention effect[11] or cellular internalization[12] of the reporter, and therefore this approach may not exploit the full potential of the targeted binding. In fact, at these late time points, even untargeted reporters such as indocyanine green are preferentially taken up by tumors.[7] There are further delivery limitations of this approach as well. First, the uptake of a fluorescent reporter, even at 24 h, is still dependent on the rate of delivery of the reporter, so it is not obvious how well it will work for more avascular tumors.[13] Second, achieving sufficient signal in the tumor at these delayed time points may require larger doses of the reporter than necessary, which could impede the clinical acceptance of these approaches. Ideally, microdose levels (<30 nmol/dose) of tracers can be used to measure uptake, which would dramatically ease the requirements for U.S. Food and Drug Administration (FDA) approval.[14] Finally, recent developments in activatable fluorescent reporters, which fluoresce only upon binding with their specific antigen, provide a means of compensating for some of these complications;[15,16] however, their uptake is still dependent on vascular permeability-mediated delivery of the reporter, and their ability to be preferentially retained at the site of activation varies with reporter type.

As a means of accounting for some of these transport-mediated aspects of targeted reporter uptake, a number of groups have investigated the employment of an untargeted reporter for referencing.[17–19] Recent work demonstrated that the simultaneous injection of an untargeted fluorescent reporter along with a targeted reporter can be used to image reporter—receptor binding *in vivo*[20] and can further be used to quantify receptor expression[21] based on "reference tissue" modeling practices.[22,23] The benefits of this approach are that any variations in reporter delivery, tissue hemodynamics, blood volume, or nonspecific uptake within a tumor or between tumor types are accounted for by measuring the uptake curve of the untargeted reporter. This enables the approach to be carried

Address all correspondence to: Kenneth M. Tichauer, Thayer School of Engineering, Dartmouth College, 8000 Cummings Hall, Hanover, New Hampshire 03766. Tel: +1 603 646 9765; Fax: +1 603 646 3856; E-mail: kenneth.tichauer@dartmouth.edu

0091-3286/2012/$25.00 © 2012 SPIE

out immediately after reporter injection, when the amount of fluorescence signal in the tissue is at a maximum, thereby enabling the lowest concentrations of reporters to be administered. The downside to the approaches demonstrated thus far[20,21] is that they require continuous monitoring of the uptake curves of both reporters over tens of minutes, which would not be ideal for translation to fluorescence-guided surgery.

In this study, a simplified version of this approach is presented with a focus on achieving optimal tumor-to-background contrast at single time points by essentially taking the ratio of the uptake images of the two reporters: one untargeted and, for investigational purposes, one targeted to epidermal growth factor receptor (EGFR), a cell surface receptor that is overexpressed in many forms of cancer.[24] This single timeframe imaging of the processed image was hypothesized to have enhanced contrast as well as be closely related to the EGFR expression activity of the tumor.

2 Materials and Methods

2.1 *Dual-Reporter Model*

Using a two-tissue compartment model to approximate the tissue distribution of the targeted imaging reporter and a one-tissue compartment model to approximate the tissue distribution of the untargeted reporter (Fig. 1), it is possible to demonstrate that the ratio of uptake of the two reporters at any given time point is proportional to the receptor density of the tissue interest. Specifically, the concentration of the targeted imaging reporter in a region of interest was modeled as a sum of the concentration of the reporter in the blood and in two tissue compartments: the blood plasma concentration, C_p; the unbound or nonspecifically bound concentration in the interstitial space, C_f; and the concentration of reporter attached to its specific receptor, C_b. Additionally, the concentration of the untargeted reporter was modeled as a sum of the blood plasma concentration, C_p, and the unbound or nonspecifically bound concentration in the interstitial space, C_r. These relationships can be expressed by the following equations if both reporters are assumed to have the same plasma curves:

$$\mathrm{ROI}_T(t) = C_p(t) + C_f(t) + C_b(t) \quad \text{and} \tag{1}$$

$$\mathrm{ROI}_{\mathrm{UT}}(t) = C_p(t) + C_r(t), \tag{2}$$

where $\mathrm{ROI}_T(t)$ and $\mathrm{ROI}_{\mathrm{UT}}(t)$ are the measured region of interest concentrations of the targeted and untargeted reporters, respectively, as a function of time t. Taking the difference between Eqs. (1) and (2) and then dividing by Eq. (2) (i.e., subtracting the untargeted reporter uptake image from the targeted image and dividing by the untargeted image) produces the following expression:

$$\frac{\mathrm{ROI}_T(t) - \mathrm{ROI}_{\mathrm{UT}}(t)}{\mathrm{ROI}_{\mathrm{UT}}(t)} = \frac{C_f(t) + C_b(t) - C_r(t)}{C_p(t) + C_r(t)}. \tag{3}$$

If it is assumed that C_f and C_r are roughly equivalent and $C_P \ll C_r$, then Eq. (3) can be simplified to

$$\frac{\mathrm{ROI}_T(t) - \mathrm{ROI}_{\mathrm{UT}}(t)}{\mathrm{ROI}_{\mathrm{UT}}(t)} = \frac{C_b(t)}{C_f(t)}. \tag{4}$$

Depending on the tumor kinetic parameters, the assumption that $C_P \ll C_r$ may or may not be true[25]; however, by 30 min postinjection, inclusion of a typical tracer plasma concentration curve from an independent study[26] assuming a 5% tumor blood volume had a <1% effect on the ratio measured in Eq. (4) in the current study (results not shown).

If first-order kinetics are assumed, then based on the compartment model present in Fig. 1, the following relationship between C_f and C_b can be derived:

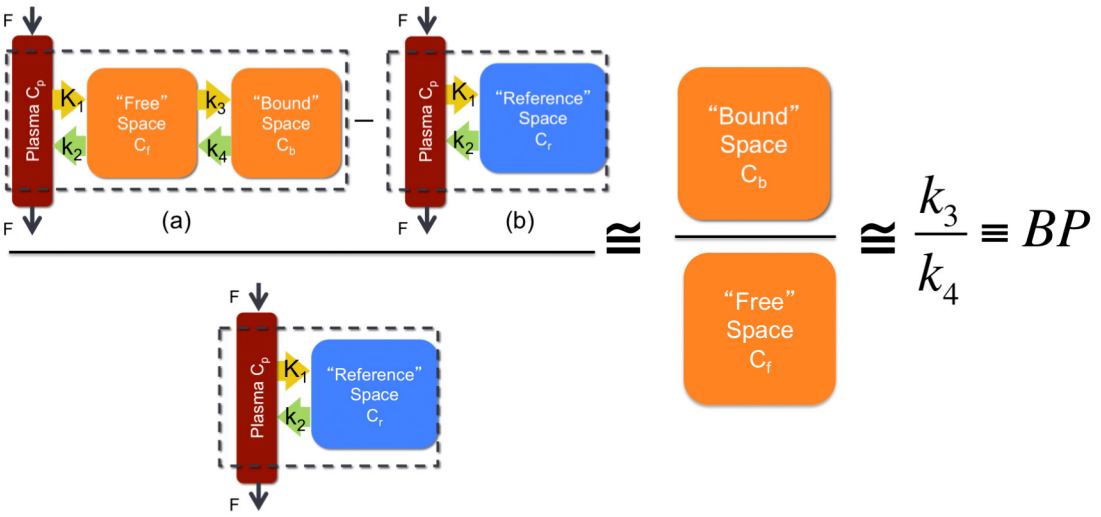

Fig. 1 An illustration of the theoretical relationship between the targeted and untargeted reporter uptake in a region of interest and the binding potential (BP: a correlate of receptor density) is shown. The two-tissue compartment model is depicted in (a) and represents the distribution of the targeted reporter in the blood, unbound in the tissue space, and specifically bound in the tissue space. The tracer is modeled to move between the compartments governed by the rate constants K_1, K_2, K_3, and K_4. The one-tissue compartment model is depicted in (b) and represents the distribution of the untargeted reporter in the blood and unbound in the tissue space (reference space). Assuming the plasma concentration is negligible and the unbound concentrations of the targeted and untargeted reporters are equivalent, it is possible to show that ratio on the left side of the expression is approximately equivalent to the binding potential (BP), which is directly proportional to receptor availability.

$$\frac{dC_b(t)}{dt} = k_3 C_f(t) - k_4 C_b(t), \tag{5}$$

where k_3 is the rate constant governing the binding of reporter in the interstitial space to specific receptors and k_4 is the rate constant governing the separation of the bound reporter from its specific receptor back into the interstitial space. Finally, if it is assumed that after a given initial time C_b and C_f are in equilibrium (i.e., $dC_b(t)/dt = 0$), then k_3/k_4 can be substituted for C_f/C_b on the righthand side of Eq. (4):

$$\frac{\mathrm{ROI}_T(t) - \mathrm{ROI}_{\mathrm{UT}}(t)}{\mathrm{ROI}_{\mathrm{UT}}(t)} = \frac{k_3}{k_4} \equiv \mathrm{BP}, \tag{6}$$

where k_3/k_4 is, by definition, the binding potential, BP, which is equal to the product of the affinity of the targeted reporter for its receptor and the receptor density.[27] Because the ratio on the left-hand side of Eq. (6) is proportional to the binding potential, it follows that contrast in a dual-reporter image is driven by the level of expression of the targeted receptor and not other factors such as hemodynamic delivery of the reporter or the amount of reporter injected.

2.2 *Animal Experiments*

To investigate the potential of the proposed dual-reporter imaging approach for improving tumor discrimination, a study was conducted on 32 immune-deficient SCID mice (Charles River, Wilmington, MA). Twenty-six-week-old mice were inoculated with a human neuronal glioblastoma (U251; supplied from Dr. Mark Israel, Norris Cotton Cancer Center, Dartmouth-Hitchcock Medical Center), a cancer cell line known to express moderate levels of EGFR;[28,29] another six mice were inoculated with a human epidermoid carcinoma (A431; ATCC, Manassas, VA), known to express a very large amount of EGFR;[30] and the final six mice were inoculated with a rat gliosarcoma (9L-GFP; supplied by Dr. Bogdanov, Dartmouth Medical School), a cell line known to express very little EGFR.[28] In all cases, the tumors were introduced by injecting 1×10^6 tumor cells in Matrigel® (BD Biosciences, San Jose, CA) into the subcutaneous space on the left thigh of the mice. The tumors were then allowed to grow to a size of approximately 150 mm^3 before imaging (roughly 2 weeks). For imaging, the mice were separated into two larger groups. In the first group, which included nine U251 mice, six 9L-GFP mice, and six A431 mice, the uptake of both an untargeted fluorescence reporter (carboxylate form of the IRDye 700DX NHS Ester; LI-COR Biosciences, Lincoln, NE) and an EGFR-targeted fluorescence reporter (IRDye 800CW EGF; LI-COR Biosciences, Lincoln, NE) was imaged at approximately 5-min intervals in the first hour after intravenous injection. In the second group, which included the remaining 11 U251 mice, the uptake of the two reporters was imaged at a single time point 24 h after reporter injection. In the first group, three of the U251 mice were injected with the fluorescent reporter cocktail 15 min after a 30-nmol (100 mL PBS) intravenous injection of free human recombinant EGF (Millipore, Temecula, CA) to carry out a blocking study (negative control). This was repeated for five of the mice in the 24-h imaging protocol, and these mice are referred to as "U251 Block" in the figures. To account for intensity differences due to quantum yield and relative reporter concentrations, as well as imaging efficiency differences at the two wavelength bands, for the two reporters, the untargeted fluorescence images at all time points were multiplied by the ratio of targeted to untargeted fluorescence measured from the injected fluorescent cocktail using the imaging system.

2.3 *Imaging Protocol*

Just before imaging, the mice were anesthetized with ketamine-xylazine (100:10 mg/kg i.p.), and the superficial tissue surrounding the tumors was removed. Each mouse was then placed tumor side down on a glass slide and loosely secured with surgical tape. Once plated, the mice were positioned onto the imaging plane of an Odyssey Scanner (LI-COR Biosciences, Lincoln, NE). The Odyssey Scanner employs raster scanning and two lasers (emitting at 685 and 785 nm) to excite the targeted and untargeted fluorophores simultaneously, pixel by pixel, and uses a series of dichroic mirrors to decouple fluorescence from the LI-COR 700-nm fluorescent reporter and the LI-COR 800-nm fluorescent reporter.

2.4 *Image Analysis*

A major purpose of this study was to compare the tumor contrast attainable with the dual-reporter approach to a conventional fluorescence-guided surgery approach that achieves contrast through targeted fluorescence uptake alone. To accomplish this, contrast was quantified by calculating the average signal in the tumor and subtracting the average signal in the skin. Then this contrast value was divided by the standard deviation (SD) of signal in the skin to estimate contrast-to-noise ratio (CNR). This calculation can be displayed mathematically as follows:

$$\mathrm{CNR}(t) = \frac{S_{\mathrm{tu}}(t) - S_{\mathrm{sk}}(t)}{\sigma_{\mathrm{sk}}(t)}, \tag{7}$$

where $S_{\mathrm{tu}}(t)$ is the average signal measured in the tumor, $S_{\mathrm{sk}}(t)$ is the average signal in the skin, and $\sigma_{\mathrm{sk}}(t)$ is the SD of the signal in the skin at time t. Figure 2 demonstrates the utility of CNR over the tumor-to-background ratio typically used to evaluated fluorescence images. The figure depicts two simulated signal profiles transecting two regions, a background region and a tumor region (given positive contrast), from a theoretical image. It is obvious from the figure that the location of the tumor is considerably more apparent in the red profile than the blue profile; however, both profiles exhibit the same tumor-to-background ratio (tumor signal/background signal) of 11. On the other hand, the CNR is 16.0 for the red profile and 1.6 for the blue profile, showing that CNR better represents the ability to visually discriminate contrast in an image.

A receiver operating characteristic (ROC) curve analysis was also carried out to further investigate the strength of each imaging approach for localizing a tumor. It was completed on an image-by-image basis for both the targeted fluorescence images and the dual-reporter images in all unblocked U251 mice at 1 and 24 h postinjection. The ROC was automated by setting the upper threshold in each image to the maximum pixel value in the image and adjusting the lower threshold incrementally by 5% of the maximum value from zero up to the maximum pixel value. At each increment, every pixel of the image was characterized as follows: if it was part of the tumor, it was recorded as a true positive (TP) if its value was greater than the lower threshold and a false positive (FP) if its value was less than the lower threshold. Conversely, if the pixel was not part of the tumor,

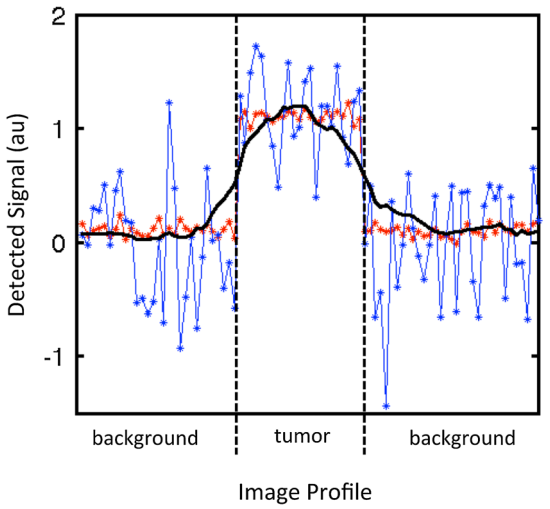

Fig. 2 Two theoretical signal profiles of an image composed of background tissue and a tumor are displayed. Both profiles demonstrated a contrast of 1 or a contrast-to-background ratio of 11, but owing to large differences in noise characteristics, the location of the tumor is much easier to see in the red profile with a contrast-to-noise ratio (CNR) of 16.0 than in the blue profile with a CNR of 1.6. A CNR profile from the dual-reporter image displayed in Fig. 5(f) is also presented as a solid black line for comparison.

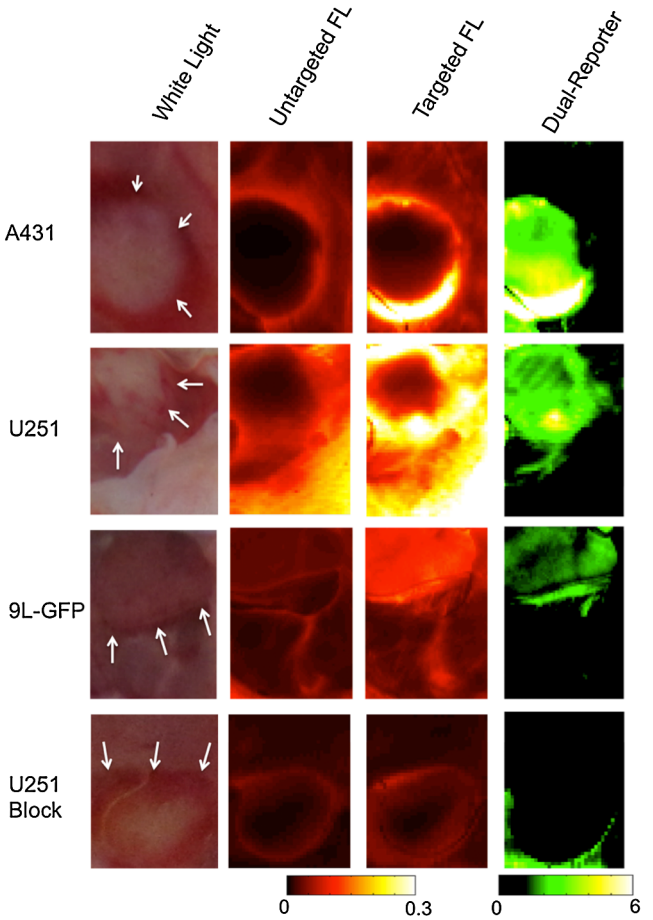

Fig. 3 Fluorescence and dual-reporter images at 1 h after dual-reporter injection. Columns 1 to 4 display a typical preimaging white light picture and corresponding untargeted fluorescence uptake (IRdye 700DX), targeted fluorescence uptake (EGF-IRdye 800CW), and dual-reporter images of each tumor line (row 1 = *A*431, row 2 = *U*251, row 3 = 9*L*-GFP, and row 4 = blocked U251), respectively. The location of the tumor is highlighted for each case on the white-light image by the dashed yellow line.

it was recorded as a false negative (FN) if its value was greater than the lower threshold and a true negative (TN) if its value was less than the lower threshold. The location of the tumor was determined from white-light images taken of the mouse before imaging. Following this characterization, the standard principles of ROC analysis were employed. Specifically, for each image the sensitivity $= \mathrm{TP}/(\mathrm{TP}+\mathrm{FN})$ and specificity $= \mathrm{TN}/(\mathrm{FP}+\mathrm{TN})$ were calculated at each threshold and ROC curves were created (sensitivity versus 1—specificity). Finally, the area under the ROC curve was calculated for all images to estimate the accuracy of the targeted fluorescence uptake and dual-reporter approaches for correctly identifying tumor over normal tissue.

2.5 *Statistics*

All statistical analyses were carried out with the statistical software package, SPSS (IBM®, Armonk, NY). For temporal analyses, a mixed two-way repeated-measures ANOVA with time as the within-subject variable and tumor group as the between-subject factor was employed. A two-way mixed ANOVA with Bonferroni correction was used to analyze tumor contrast-to-noise for each imaging method and at each imaging time point after reporter injection. Linear regression was employed to compare dual-reporter results with *in vivo* binding potentials.[21] Statistical significance was based on $P < 0.05$. All data are presented as mean $\pm$ SD unless stated otherwise.

3 Results

Figrue 3 presents representative targeted and untargeted fluorescence images, as well as the corresponding white-light image and a dual-reporter image, in each tumor group at 1 h after intravenous injection of a mixture of EGFR-targeted and untargeted fluorescent reporters (fluorescing at 800 and 700 nm, respectively). In a strictly qualitative sense, for the two tumors that are known to express EGFR (A431 and U251), it was easier to locate the tumor using the dual-reporter image [from Eq. (6)] than with the targeted or untargeted fluorescence images alone at 1 h. Figure 4 elaborates on these observations, presenting a more quantitative analysis. In Fig. 4(a), the average CNRs of targeted fluorescence uptake in A431, U251, 9L-GFP, and blocked U251 tumors are depicted within 1 h after injection of the dual-reporter mixture. A repeated-measures mixed ANOVA demonstrated a significant two-way effect in the data in the form of a significant time-by-tumor line effect ($P < 0.01$). This suggested that the dynamics of the tumor lines were significantly different; in particular, the U251 tumors tended to exhibit a quicker release of the targeted reporter after injection than the other groups. Despite this effect, however, the between-subject omnibus test suggested that uptake differences were not significant between the tumor lines, at any time point in any tumor line, and no correlation was found between targeted fluorescence uptake and the expected magnitude of EGFR expression in the different tumor lines at any time point. On the other hand, the time courses of the dual-reporter tumor CNRs [depicted in Fig. 3(b)] demonstrated a clear ability to resolve the location of the tumor using dual-reporter imaging

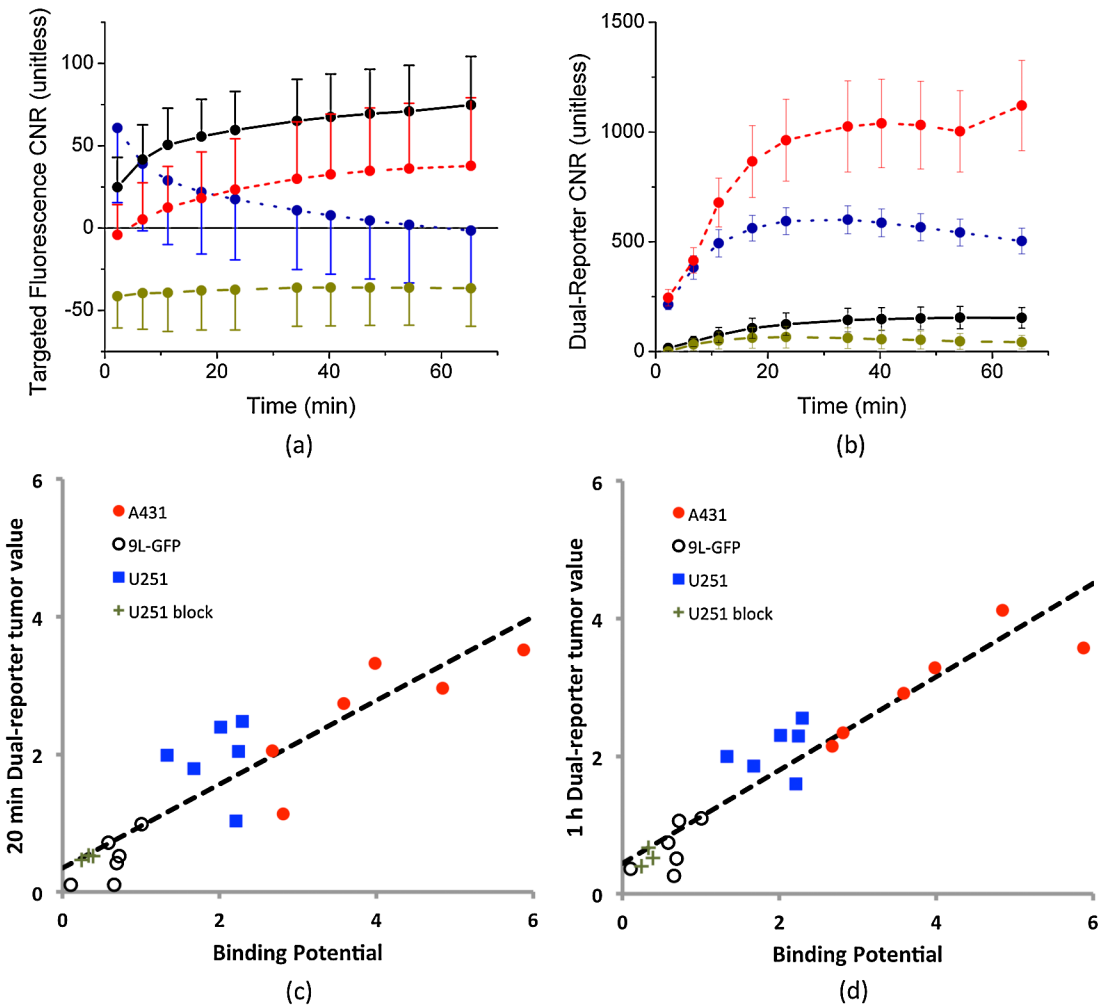

Fig. 4 Targeted fluorescence uptake versus dual-reporter imaging within 1 h of reporter injection. The mean ± standard error targeted fluorescence uptake tumor contrast-to-noise ratio (CNR) within 1 h of reporter injection is presented in (a) for each tumor group (*A*431 = red; *U*251 = blue; 9*L*-GFP = black; blocked U251 = dark yellow). The mean ± standard error tumor CNR determined by the dual-reporter approach for the same tumor groups as in (a) is presented in (b). The correlation between the average dual-reporter image value of the tumor in each mouse at 20 min and 1 h after reporter injection and the corresponding binding potential (an *in vivo* marker of receptor expression) are presented in (c) and (d), respectively. Data points from each tumor line are color-coded to match the data in (a) and (b). The slope of the 20-min correlation was 0.61 ± 0.12 ($r = 0.89$, $P < 0.05$), and the 1-h correlation was 0.68 ± 0.05 ($r = 0.94$, $P < 0.01$).

at all time points after injection (even at 1 min) for the U251 and A431 tumor lines, and by 20 min after reporter injection for the 9L-GFP tumor line ($P < 0.001$). The dual-reporter image CNR of the blocked U251 tumors never reached a level of significance over the background. Moreover, by 20 min, the average dual-reporter image value in the tumor [Eq. (6)] measured in each tumor group was significantly different from all other tumor groups, and the difference correlated with the expected differences in EGFR expression between the groups. More specifically, at 20 min, the average tumor dual-reporter CNR in the blocked U251 line, expected to express the least amount of EGFR, was 67 ± 59; in the 9L-GFP line, expected to express a little amount of EGFR, was 116 ± 49; in the U251 line, expected to express a moderate level of EGFR, was 578 ± 59; and in the A431 line, expected to express the most EGFR of the tumor lines, was 922 ± 172. To investigate this relationship further, correlation plots were created relating the dual-reporter tumor value at 2 min [Fig. 4(c)] and 1 h [Fig. 4(d)] to the *in vivo* binding potential, a quantitative marker of receptor expression that has been validated against *ex vivo* and *in vitro* measures.[21] This approach takes as input the full temporal uptake curve of the targeted and untargeted reporters in the first hour after injection and employs a simplified reference tissue model[22] to measure binding potential using the uptake of the untargeted reporter as a "reference tissue." A statistically significant correlation was observed between the two measures at 20 min and 1 h, with slopes of 0.61 ± 0.12 ($P < 0.05$, $r = 0.89$) and 0.68 ± 0.05 ($P < 0.01$, $r = 0.94$), respectively.

Although the dual-reporter approach demonstrated obvious improvements over targeted fluorescence uptake alone for the localization of EGFR-expressing cancerous tissue, fluorescence uptake is generally measured at much longer time points after injection because of the known lack of sensitivity at early time points.[31] For comparison, targeted and untargeted fluorescence uptakes were also measured in a separate set of U251 and blocked U251 mice at a single time point 24 h after reporter injection. Figure 5(a) shows a box-plot of the targeted fluorescence uptake at both 24 h and 1 h for the U251 and blocked U251 groups. As demonstrated by the plot, the only group that presented an average tumor CNR that was significantly

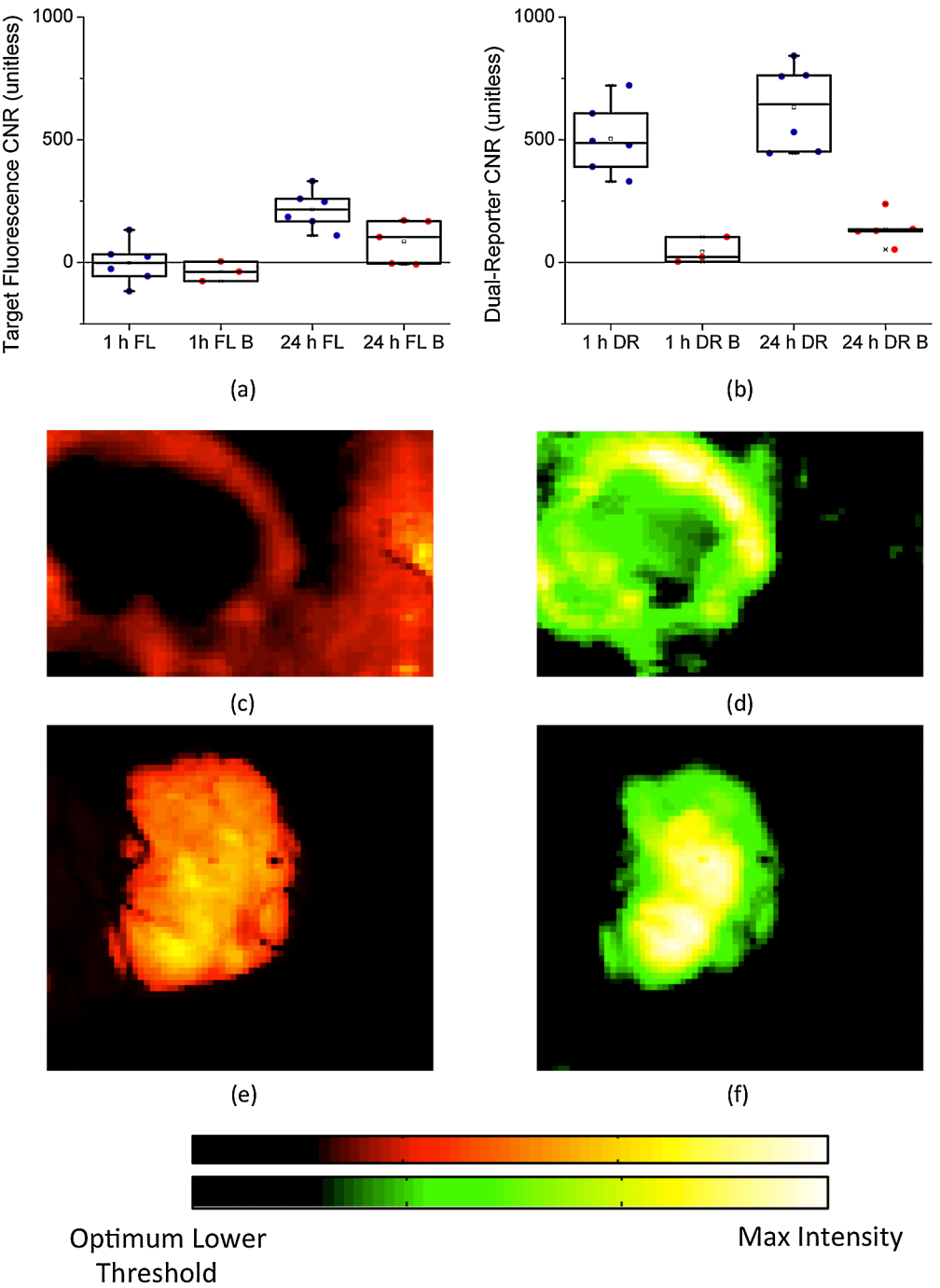

Fig. 5 Tumor contrast-to-noise ratio (CNR) comparison is shown between targeted fluorescence uptake and dual-reporter images. A box-plot of the tumor CNR determined from targeted fluorescence uptake images at 1 and 24 h after reporter injection in mice with blocked (FL B) and unblocked (FL) U251 tumors are presented in (a). Each data point represents an individual average tumor CNR from one mouse. Blue data points represent measurements taken in unblocked U251 tumors and red data points represent measurements taken in blocked U251 tumors. A similar box plot is presented in (b), with the tumor CNR determined from the dual-reporter (DR) images at 1 and 24 h after reporter injection. Examples of the targeted fluorescence uptake images at 1 and 24 h are presented in (c) and (e), respectively, and examples of the dual-reporter images at 1 and 24 h are presented in (d) and (f). The maximum value in each image was chosen as the maximum threshold of the color scale, and the lower threshold was chosen independently in each image by a receiver operating characteristic analysis to optimize the tumor CNR in each case.

different from zero ($p < 0.001$)—i.e., measurable from the background—was the fluorescence at 24 h in the unblocked U251 group, with a CNR of 217 ± 78. For comparison, Fig. 5(b) displays dual-reporter tumor CNR data for the same groups as in Fig. 5(a). For this measure, the tumor CNRs of both the 1- and 24-h dual-reporter values in the unblocked U251 mice were significantly different from zero ($P < 0.001$), whereas the dual-reporter value in the blocked groups was not. The average dual-reporter tumor CNR at 1 h was 503 ± 58, and at 24 h was 631 ± 175 (there was no statistically significant difference between these). Of note, the dual-reporter tumor CNR was significantly higher than the targeted fluorescence CNR at 24 h ($P < 0.01$). Examples of the targeted fluorescence uptake image and the dual-reporter image from a single U251

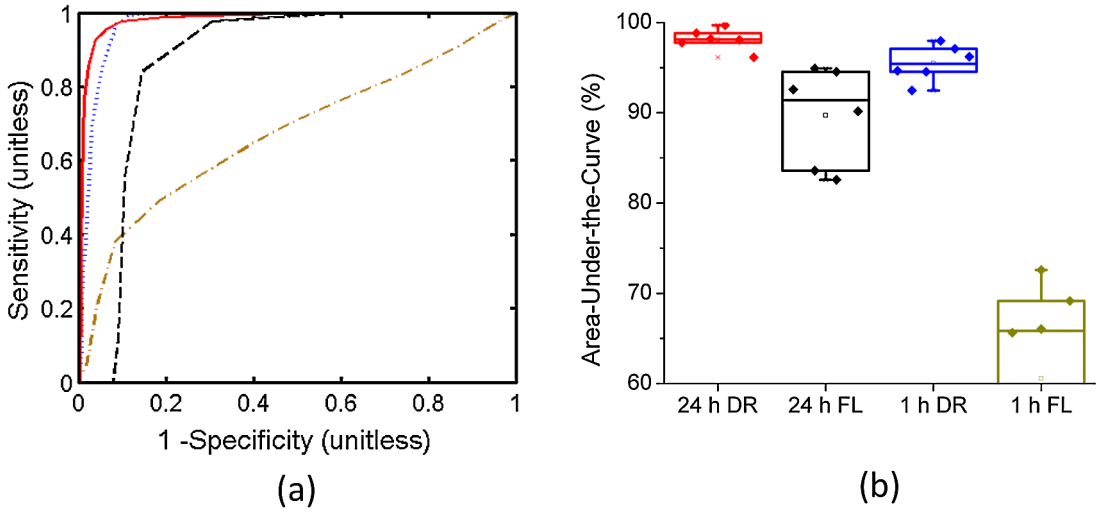

Fig. 6 Receiver operating characteristic (ROC) analysis was used, where typical ROC curves for the dual-reporter approach at 1 h after reporter injection (blue line) and 24 h after injection (red line), and for the targeted fluorescence uptake approach at 1 h after injection (dark yellow line) and 24 h after injection (dashed black line) are presented in (a) for a 1-h U251 mouse and a 24-h U251 mouse. The areas-under-the-curve (approximate accuracies) of each ROC curve for all U251 mice at 1 and 24 h using the targeted fluorescence uptake approach (FL) and the dual-reporter approach (DR) are displayed in boxplots in (b). The color-coding matches that in (a). Each data point corresponds to an independent accuracy measurement for a single mouse using a single approach.

mouse at 1 h after reporter injection are presented in Fig. 5(c) and 5(d), respectively, and examples from a single U251 mouse at 24 h after reporter injection are presented in Fig. 5(e) and 5(f). The maximum value in each image was chosen as the maximum threshold of the color scale, and the lower threshold was chosen independently in each image by ROC analysis to optimize the tumor CNR in each case and observe the ultimate potential of each approach.

A more in-depth analysis of the benefits of dual-reporter imaging over targeted fluorescence alone is presented in Fig. 6. In Fig. 6(a), typical ROC curves for the different approaches of localizing cancerous tissue (targeted fluorescence uptake or dual-reporter imaging at 1 or 24 h after reporter injection) are presented for U251 mice. By applying the area-under-the-curve analysis to each cancer localization approach for each mouse, the average accuracy of the targeted fluorescence uptake approach was estimated to be 60% ± 13% and 90% ± 5% at 1 and 24 h after reporter injection, respectively. The average accuracy of the dual-reporter approach was 96% ± 2% and 98% ± 1% at 1 and 24 h after reporter injection. The improved accuracy of the dual-reporter approach at 1 and 24 h postinjection over the targeted fluorescence uptake approach at 24 h was statistically significant ($P < 0.001$ for the 24-h dual-reporter approach compared to 24-h fluorescence uptake and $P < 0.05$ for the 1-h dual-reporter approach compared to the 24-h fluorescence uptake).

Fluorescence uptake in the kidney of targeted and untargeted reporters was visible in 3 of the 6 24-h U251 mice [Fig. 7(a) and 7(b)]. As the kidney is the major filtering organ of these reporters, signal from the kidney can be a significant source of non-receptor-mediated fluorescence uptake.[32] To avoid potential bias, the kidney was not included in the ROC analyses presented in Fig. 6; however, it is a strength of the dual-reporter approach that the kidney, although dominant in the targeted and untargeted fluorescence uptake images, was not visible in the dual-reporter images [Fig. 7(c)]. Image thresholds for Fig. 7 were selected based on optimal thresholds from ROC analyses of each image, independently.

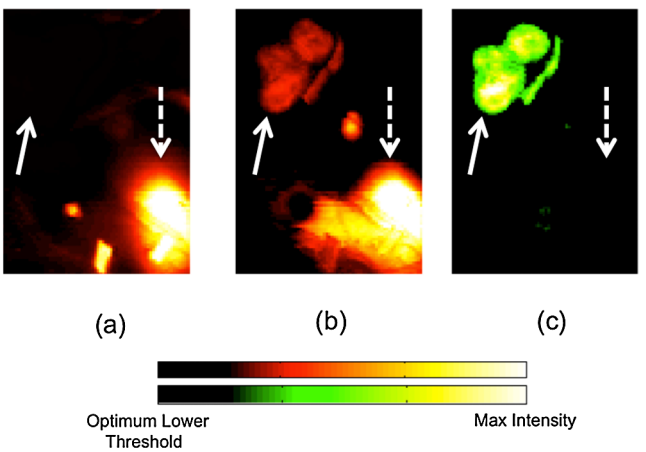

Fig. 7 Qualitative specificity of targeted fluorescence uptake and dual-reporter approaches for localizing cancerous tissue is shown. Examples of an untargeted fluorescence uptake image (a) and a corresponding targeted fluorescence uptake image (b) and dual-reporter image (c) at 24 h in a U251 mouse are presented. The solid white arrow points to the location of the tumor, and the dashed white arrow points to the location of a kidney. Images are thresholded to optimize tumor localization based on a receiver operating characteristic analysis.

4 Discussion

Use of fluorescence-guided surgery (FGS) in oncology has been limited, yet is growing in applications. Typically, receptor-mediated guidance would involve three steps. The first step would be systemic administration of the fluorescent molecule that is targeted to a cancer-specific receptor (e.g., EGFR). The second step would be to wait for the fluorescence to be carried by the blood throughout the body, and then, importantly, to wait for the washout of any nonspecific uptake of the targeted fluorescence to ensure that the tumor-to-background CNR is maximal for tumor delineation. The third step would then be the surgery, removing any suspicious tissue that is highlighted

by abnormally high fluorescence uptake. The problem with this approach is that the uptake of a targeted reporter in a specific region of interest is not just governed by that region's targeted receptor expression; other physiological factors play roles as well, such as blood flow, vessel permeability, cellular internalization, interstitial pressure, and other nonreceptor-mediated mechanisms of reporter uptake and retention.[33] Therefore a cancerous lesion with a low blood supply or a high interstitial pressure may exhibit low fluorescence uptake despite overexpressing the targeted receptor or an organ that acts to filter agents from the bloodstream (kidney, liver, spleen) may have substantial fluorescence uptake despite expressing no specific receptor. At this early time in the development of fluorescence guidance, it is still not clear if bulk uptake of reporter might have advantages over binding assay reporters; however, it is clearly true that most conventional approaches to this problem have not been able to attribute their signal uniquely to binding alone. This study presents a dual-reporter imaging approach that was designed to mitigate the nonreceptor-mediated effects of targeted reporter uptake by accounting for them with the measurement of a simultaneously injected untargeted fluorescence reporter. Fluorescence was imaged on an Odyssey system, which is a flat-panel scanner, incapable of use during surgery. This system was employed to study the potential for dual-reporter imaging to be done, since it is optimized to eliminate cross-talk between concentrations of the two LI-COR fluorescent reporters used. Further studies are ongoing to test out the approaches of this study using a hyperspectral fluorescence surgical microscope.

In Sec. 2, an expression was derived, building upon earlier work,[20] relating the uptake of a targeted imaging reporter and an untargeted reporter in a region of interest with the binding potential in that region (a parameter directly proportional to the targeted receptor density[27]). To investigate the utility of this approach, the uptakes of the two fluorescent reporters (one targeted to EGFR and one untargeted) were tracked over the first 1 h after injection in four tumor groups (A431, U251, 9L-GFP, and U251 blocked) and at 24 h in U251 and U251 blocked groups. The results were used to compare the dual-reporter approach against conventional targeted fluorescence uptake imaging with regard to tumor discrimination.

There were two salient findings of the current study. The first was that the dual-reporter approach for tumor discrimination, when applied at 1 or 24 h after reporter injection, was superior at discriminating the tumor compared to the more conventional approach of measuring targeted fluorescence uptake alone at 1 and 24 h postinjection (Figs. 5 and 6), in terms of both tumor-to-background CNR and area under the ROC curve. This is a major finding, since surgical guidance by targeted fluorescence alone has been highly touted to improve the success rate of tumor resections, and this study suggests that employing a dual-reporter approach can improve the ability to discriminate between tumor and healthy tissue even further. Moreover, because the dual-reporter approach is so successful at relatively early times after reporter injection (1 h), it could require lower dosages of imaging reporters, which may improve the potential for new reporters to gain clinical approval.[34] Additionally, the signal attained at these early points is more likely to be driven by targeted receptor availability as opposed to longer-term effects such as cellular internalization. If the goal is simply to discriminate between tumor and healthy tissue, though, cellular internalization may actually improve the contrast, as seen by the fact that the 24-h dual-reporter images were roughly equivalent in performance to the 1-h dual-reporter images despite having poorer signal-to-noise characteristics because of prolonged fluorescence washout (the SNR in the fluorescence images was approximately 3 times higher at 1 h than at 24 h). However, if the goal is also to estimate the level of targeted receptor expression, the influence of cellular internalization should be avoided, since this will cause the receptor expression to be overestimated (the average dual-reporter value in U251 tumors was 3.5 ± 0.3 at 1 h after fluorescence injection and 10.6 ± 1.2 at 24 h). An interesting caveat to the dual-reporter images is that they are not as affected by signal contamination in organs of filtration. The reporters used in this study are less than 5.5 nm in diameter and are therefore preferentially filtered by the kidney.[35,36] Significant untargeted and targeted fluorescence signal from the kidney was evident in three of the 24-h mice; however, since the uptake of the two reporters was relatively equivalent, any signal from the kidney was normalized out in the dual-reporter images (Fig. 7). The upshot of this is that the dual-reporter approach could make it possible to localize tumors that are proximal to organs of filtration, a feat that would be very difficult using targeted fluorescence uptake alone.

The second salient finding of this study was that by 20 min after reporter injection, the dual-reporter approach demonstrated a statistically significant correlation with a more robust *in vivo* measure of the binding potential that employed fitting the full time courses of fluorescence uptake of both reporters [Fig. 4(c)]. This robust binding potential measure makes fewer physiologic assumptions than the dual-reporter approach and has been validated in a previous study against *ex vivo* and *in vitro* measures of receptor density.[21] Although it represented a strong correlation, the slope of the regression was significantly different from 1 (0.68 ± 0.05), probably because there is approximately 10 times greater autofluorescence in the 700-nm (untargeted) fluorescence channel than in the 800-nm (targeted) fluorescence channel. This would lead to an overestimation of the untargeted fluorescence uptake, and from Eq. (6), it can be seen that this overestimation will lead to an underestimation in the numerator and an overestimation in the denominator, compounding to cause a magnified underestimation in the single time point—derived binding potential. It is possible to account for the increased autofluorescence in the 700-nm channel by collecting a pre-reporter injection scan, which can be subtracted from subsequent scans. However, in the field of fluorescence-guided surgery where the imaging field could be constantly changing, it would be better to develop an approach that would be insensitive to motion. Indeed, the strength of the correlation between the dual-reporter value and binding potential presented in Fig. 3(c), which was significant from 20 min on, demonstrates that this approach has the potential to provide a real-time, motion-insensitive measure of receptor density and therefore can discriminate between tissues based on receptor density, and receptor density alone.

Activatable fluorescence reporters that do not fluoresce unless bound to a specific receptor of interest constitute another approach to amplify receptor density—derived contrast in FGS.[6,16] Because these reporters provide contrast only where activator is present, many of the factors that involve nonreceptor-mediated reporter uptake and could confound conventional FGS are avoided; however, the contrast is still founded on reporter binding as opposed to receptor density as with the

dual-reporter approach. This means that the amount of activated fluorescence is still influenced, perhaps strongly, by the hemodynamics, vascular permeability, and interstitial pressure of the region of interest, all of which can vary substantially both between and within tumors.[37] The proposed dual-reporter approach avoids these factors by essentially referencing the uptake of the targeted reporter to the untargeted reporter. Therefore, the sensitivity of this approach is predominantly governed by the dynamic range of the imaging modality used to detect the fluorescence. In other words, if the assumptions of the dual-reporter theory hold, the approach is only susceptible to fluorescence detection saturation or areas with a limited SNR, which could occur in areas of necrosis.

Reiterating the Methods, the dual-reporter expression relating the uptake of the targeted and untargeted reporters with the level of receptor expression [Eq. (6)] relies on the following assumptions: that the plasma and free-space components of the respective reporter concentrations in tissue are roughly equivalent, that the bound and unbound states of the targeted reporter are in an instantaneous equilibrium (i.e., the adiabatic approximation holds[22]), that the tissue concentration of the untargeted reporter is predominantly composed of reporter in the extravascular space (i.e., the plasma component is approximately negligible or equivalent in all cases), and that the targeted tracer concentration is considerably less than the receptor concentration to avoid receptor saturation effects. The strength of the results in the current study suggests that each of these assumptions is adequate; however, further investigation is necessary to fully characterize the utility of the presented FGS technique. In a previous study, the plasma curves of IRDye 800CW-EGF and IRDye 700DX (the targeted and untargeted agents used in this study) were found to be very similar in immune-compromised mice, being approximated by exponential decay functions with half-lives of approximately 8 min,[26] and studies are ongoing to investigate the reliability of the other model assumptions under different physiological conditions (nonspecific binding and cellular internalization) using a full kinetic forward model. Furthermore, we are investigating the potential of employing an enantiomer of the targeted reporter as an untargeted reporter to minimize any differences between the two. For example, for EGFR targeting it would be possible to use an anti-EGFR Affibody® imaging agent for the targeted reporter and a negative control Affibody imaging agent for the untargeted reporter.[38,39] With respect to receptor saturation, it may be possible to include second-order kinetics in the model to account for this;[40] however, keeping injected fluorescence at tracer levels (i.e., far below receptor saturation) will likely be important for clinical translation. In a previous study, we demonstrated that a 1-nmol dose of IRDye 800CW-EGF in mice would be far below saturation levels for a tumor of similar EFGR expression.[26] Another factor that can also affect the efficacy of the dual-reporter approach is the influence of specific uptake from other organs. More specifically, the technique requires that the tumor of interest expresses significantly more of the targeted receptor than the surrounding tissue. This could be a problem for EGFR targeting, for example, if the tumor is proximal to an organ like the pancreas, which is known to express a significant amount of EGFR.[26,41]

In conclusion, the current study introduces a novel fluorescence-guided surgery technique that utilizes a secondary, untargeted imaging reporter to account for nonreceptor-mediated uptake of the targeted fluorescence. This dual-reporter approach was demonstrated to provide instantaneous maps that could be used to discriminate between cancerous and healthy tissue with significantly better contrast-to-noise and ROC analysis characteristics than targeted fluorescence uptake alone. Furthermore, by 20 min after injection of the fluorescent reporters, the average dual-reporter image values in a range of tumor types demonstrated a significant correlation with tumor binding potential (a measure of receptor expression). Therefore, not only does the dual-reporter approach outperform conventional fluorescence intensity imaging for tumor/healthy tissue discrimination, but it also provides an estimate of tumor receptor status, which could be used to inform the choice or progress of biological therapies that target the same receptors.[10,42]

Acknowledgments

This research was funded by NIH grants P01CA84201, R01CA156177, and U54CA151662. K. M. Tichauer acknowledges funding from the Canadian Institutes of Health Research postdoctoral fellowship program.

References

1. S. Gioux, H. S. Choi, and J. V. Frangioni, "Image-guided surgery using invisible near-infrared light: fundamentals of clinical translation," *Mol. Imag.* **9**(5), 237–255 (2010).
2. B. W. Pogue et al., "Review of neurosurgical fluorescence imaging methodologies (vol. 16, pg 493, 2010)," *IEEE J. Sel. Top. Quant.* **16**(6), 1847–1847 (2010).
3. D. W. Roberts et al., "Coregistered fluorescence-enhanced tumor resection of malignant glioma: relationships between delta-aminolevulinic acid-induced protoporphyrin IX fluorescence, magnetic resonance imaging enhancement, and neuropathological parameters," *J. Neurosurg.* **114**(3), 595–603 (2011).
4. W. Stummer et al., "Fluorescence-guided surgery with 5-aminolevulinic acid for resection of malignant glioma: a randomised controlled multicentre phase III trial," *Lancet Oncol.* **7**(5), 392–401 (2006).
5. S. L. Troyan et al., "The FLARE intraoperative near-infrared fluorescence imaging system: a first-in-human clinical trial in breast cancer sentinel lymph node mapping," *Ann. Surg. Oncol.* **16**(10), 2943–2952 (2009).
6. G. M. van Dam et al., "Intraoperative tumor-specific fluorescence imaging in ovarian cancer by folate receptor-alpha targeting: first in-human results," *Nat. Med.* **17**, 1315–1319 (2011).
7. N. Kosaka et al., "Near infrared fluorescence-guided real-time endoscopic detection of peritoneal ovarian cancer nodules using intravenously injected indocyanine green," *Int. J. Cancer* **129**(7), 1671–1677 (2011).
8. E. M. Sevick-Muraca et al., "Imaging of lymph flow in breast cancer patients after microdose administration of a near-infrared fluorophore: feasibility study," *Radiology* **246**(3), 734–741 (2008).
9. N. Tagaya et al., "Intraoperative identification of sentinel lymph nodes by near-infrared fluorescence imaging in patients with breast cancer," *Am. J. Surg.* **195**(6), 850–853 (2008).
10. R. Weissleder and M. J. Pittet, "Imaging in the era of molecular oncology," *Nature* **452**(7187), 580–589 (2008).
11. H. Maeda et al., "Tumor vascular permeability and the EPR effect in macromolecular therapeutics: a review," *J. Control. Release* **65**(1–2), 271–284 (2000).
12. R. K. Jain, "Transport of molecules, particles, and cells in solid tumors," *Annu. Rev. Biomed. Eng.* **1**, 241–263 (1999).
13. J. W. Baish et al., "Role of tumor vascular architecture in nutrient and drug delivery: an invasion percolation-based network model," *Microvasc. Res.* **51**(3), 327–346 (1996).
14. G. Lappin, "Microdosing: current and the future," *Bioanalysis* **2**(3), 509–517 (2010).
15. V. Ntziachristos et al., "Fluorescence molecular tomography resolves protease activity in vivo," *Nat. Med.* **8**(7), 757–760 (2002).

16. R. Weissleder et al., "In vivo imaging of tumors with protease-activated near-infrared fluorescent probes," *Nat. Biotechnol.* **17**(4), 375–378 (1999).
17. D. M. Goldenberg et al., "Radioimmunodetection of cancer with radioactive antibodies to carcinoembryonic antigen," *Cancer Res.* **40**(8 Pt. 2), 2984–2992 (1980).
18. K. R. Hine et al., "Radioimmunodetection of gastrointestinal neoplasms with antibodies to carcinoembryonic antigen," *Cancer Res.* **40**(8 Pt. 2), 2993–2996 (1980).
19. J. T. Liu et al., "Quantifying cell-surface biomarker expression in thick tissues with ratiometric three-dimensional microscopy," *Biophys. J.* **96**(6), 2405–2414 (2009).
20. B. W. Pogue et al., "Imaging targeted-agent binding in vivo with two probes," *J. Biomed. Opt.* **15**(3), 030513 (2010).
21. K. M. Tichauer et al., "In vivo quantification of tumor receptor binding potential with dual-reporter molecular imaging," *Mol. Imag. Biol.* (2011).
22. A. A. Lammertsma and S. P. Hume, "Simplified reference tissue model for PET receptor studies," *Neuroimage* **4**(3 Pt. 1), 153–158 (1996).
23. J. Logan et al., "Distribution volume ratios without blood sampling from graphical analysis of PET data," *J. Cereb. Blood Flow Metab.* **16**(5), 834–840 (1996).
24. C. T. Kuan, C. J. Wikstrand, and D. D. Bigner, "EGF mutant receptor vIII as a molecular target in cancer therapy," *Endocr. Relat. Cancer* **8**(2), 83–96 (2001).
25. J. Delforge et al., "In vivo quantification and parametric images of the cardiac beta-adrenergic receptor density," *J. Nucl. Med.* **43**(2), 215–226 (2002).
26. K. S. Samkoe et al., "High vascular delivery of EGF, but low receptor binding rate is observed in AsPC-1 tumors as compared to normal pancreas," *Mol. Imag. Biol.* Aug. 17, [Epub ahead of print] (2011).
27. R. B. Innis et al., "Consensus nomenclature for in vivo imaging of reversibly binding radioligands," *J. Cereb. Blood Flow Metab.* **27**(9), 1533–1539 (2007).
28. S. L. Gibbs-Strauss et al., "Detecting epidermal growth factor receptor tumor activity in vivo during cetuximab therapy of murine gliomas," *Acad. Radiol.* **17**(1), 7–17 (2010).
29. J. J. Smith, R. Derynck, and M. Korc, "Production of transforming growth factor alpha in human pancreatic cancer cells: evidence for a superagonist autocrine cycle," *Proc. Natl. Acad. Sci. USA* **84**(21), 7567–7570 (1987).
30. C. J. Wikstrand et al., "Cell surface localization and density of the tumor-associated variant of the epidermal growth factor receptor, EGFRvIII," *Cancer Res.* **57**(18), 4130–4140 (1997).
31. J. L. Kovar et al., "A systematic approach to the development agents for optical imaging of mouse of fluorescent contrast cancer models," *Anal. Biochem.* **367**(1), 1–12 (2007).
32. J. L. Kovar et al., "A systematic approach to the development of fluorescent contrast agents for optical imaging of mouse cancer models," *Anal. Biochem.* **367**(1), 1–12 (2007).
33. A. I. Minchinton and I. F. Tannock, "Drug penetration in solid tumours," *Nat. Rev. Cancer* **6**(8), 583–592 (2006).
34. J. K. Willmann et al., "Molecular imaging in drug development," *Nat. Rev. Drug Discov.* **7**(7), 591–607 (2008).
35. T. Olafsen and A. M. Wu, "Antibody vectors for imaging," *Semin. Nucl. Med.* **40**(3), 167–181 (2010).
36. H. S. Choi et al., "Renal clearance of quantum dots," *Nat. Biotechnol.* **25**(10), 1165–1170 (2007).
37. M. W. Dewhirst et al., "Morphologic and hemodynamic comparison of tumor and healing normal tissue microvasculature," *Int. J. Radiat. Oncol. Biol. Phys.* **17**(1), 91–99 (1989).
38. V. Tolmachev et al., "Imaging of EGFR expression in murine xenografts using site-specifically labelled anti-EGFR 111In-DOTA-Z EGFR:2377 Affibody molecule: aspect of the injected tracer amount," *Eur. J. Nucl. Med. Mol. Imag.* **37**(3), 613–622 (2010).
39. S. B. Lee et al., "Affibody molecules for in vivo characterization of HER2-positive tumors by near-infrared imaging," *Clin. Canc. Res.* **14**(12), 3840–3849 (2008).
40. V. Chernomordik et al., "Quantitative analysis of Her2 receptor expression in vivo by near-infrared optical imaging," *Mol. Imag.* **9**(4), 192–200 (2010).
41. M. Korc et al., "Binding of epidermal growth factor in rat pancreatic acini," *Biochem. Biophys. Res. Commun.* **111**(3), 1066–1073 (1983).
42. M. Hassan et al., "In vivo method to monitor changes in HER2 expression using near-infrared fluorescence imaging," *Mol. Imag.*, Sep 30, [Epub ahead of print] (2011).